JOURNAL OF COLLOID AND INTERFACE SCIENCE **180,** 98–105 (1996)
ARTICLE NO. 0277

Small-Angle Neutron Scattering Investigation of Supramolecular Assemblies in Ternary Systems of Alkyldimethylamine Oxide/Cinnamic Acid/Water

HIROSHI OKAMURA,* TOYOKO IMAE,*,[1] KATSUHIKO TAKAGI,† YASUHIKO SAWAKI,† AND MICHIHIRO FURUSAKA‡

*Department of Chemistry, Faculty of Science, and †Department of Applied Chemistry, Faculty of Engineering, Nagoya University, Nagoya 464, Japan; and ‡National Laboratory of High Energy Physics, Tsukuba 305, Japan

Received June 19, 1995; accepted November 13, 1995

Supramolecular assemblies in ternary systems of alkyldimethylamine oxide (C_nDAO, n = 12, 16)/cinnamic acid/D_2O were investigated by small-angle neutron scattering. In the C_{12}DAO/cinnamic acid/D_2O system, prolate ellipsoidal micelles with axial ratios of 1.3 and 2.4 were formed at mixing molar ratios X ([cinnamic acid]/[C_nDAO]) of 0 and 0.2, respectively. For the C_{16}DAO/cinnamic acid/D_2O system, lamellar layers with a bilayer thickness of 30 Å existed in a solution at X = 0, while rodlike micelles with a cross-sectional diameter of 50 Å were constructed at X = 0.2. Vesicles in solutions at X = 0.5–1 had multilamellar layers. The bilayer thickness was 23–30 and 35–36 Å for C_{12}DAO/cinnamic acid and C_{16}DAO/cinnamic acid vesicles, respectively. The thinner bilayer thickness suggests that the tilt or random orientation of alkyl chains may occur in lamellar bilayers and membrane bilayers. The comb-shaped arrangement is also possible in membrane bilayers by C_nDAO/cinnamic acid complex. © 1996 Academic Press, Inc.

Key Words: **alkyldimethylamine oxide; cinnamic acid; small-angle neutron scattering; micelle; vesicle; lamellar layer.**

INTRODUCTION

Supramolecular assemblies, which are constructed in aqueous solutions of amphiphiles, change their structures and properties on addition of cosurfactants or oil components. It has reported that different structures of molecular assemblies offer the photochemical reaction matrices which result in different reaction efficiency and stereochemical selectivity (1–3). The photodimerization reaction of aromatic unsaturated carboxylic acids proceeds in dispersions of clays and in solutions of molecular assemblies (4–7). The recent investigations were focused on finding the optimum matrix in which the specific photoreaction occurs most effectively.

Dodecyldimethylamine oxide (C_{12}DAO) is soluble in water at room temperature (~25°C) and forms small micelles (8–10). On the other hand, hexadecyldimethylamine oxide (C_{16}DAO) constructs lamellar layers in water below 30°C (11–13). Light scattering and transmission electron microscopic (TEM) investigations were carried out for the ternary systems C_{12}DAO/cinnamic acid/water and C_{16}DAO/cinnamic cid/water (14, 15). Average molecular weight, radius of gyration, and hydrodynamic radius were evaluated from static and dynamic light scattering data. The size of molecular assemblies drastically changed at the mixing molar ratio X ([cinnamic acid]/[C_nDAO]) of ~0.4. The TEM photographs displayed vesicular images with multilamellar layers for solutions at higher molar ratios.

The photoreaction of cinnamic acid in aqueous C_nDAO solutions produced different quantum efficiencies and stereochemical selectivities for cyclodimers, depending on the molecular assembly species (14). The photodimerization proceeded effectively in vesicles rather than in micelles. The dimerization yields increased with mixing ratio and were in the order syn-HT < syn-HH < anti-HH. The location and organization of cinnamic acid on the reaction matrices are expected to be associated with the structures of resultant isomeric dimers. However, such an arrangement of cinnamic acid was estimated only by speculation.

In this work, small-angle neutron scattering (SANS) was measured for the C_nDAO/cinnamic acid/water ternary systems. The fine structures of molecular assemblies were quantitatively examined for solutions with different mixing ratios. Since SANS is operated at the neutron radiation of 1–16 Å wavelength, it results in distances of nanometer scale such as the shape of small micelles, the cross section of rodlike micelles, and the lamellar thickness and distance. Such data have never been obtained from TEM and light scattering experiment (14, 15). The molecular arrangement in supramolecular assemblies is discussed in relation to the structure geometry.

[1] To whom correspondence should be addressed.

0021-9797/96 $18.00

EXPERIMENTAL

C_{12}DAO was purchased from Fluka, Chemie AG. C_{16}DAO was the same sample previously synthesized and used (14). Cinnamic acid ($C_6H_5CH = CHCOOH$) was a commercial product. D_2O (>99.75% purity) was purchased from Wako Pure Chemical Industries, Ltd. All solutions were prepared at a constant total concentration (2 mg/cm^3) of C_nDAO and cinnamic acid with different mixing ratios.

SANS measurements were carried out at room temperature on a cold neutron small-angle scattering instrument (SAN) at the National Laboratory for High Energy Physics (KEK). The SANS intensities were observed as a function of the Bragg wavenumber Q [$= (4\pi/\lambda)\sin(\theta/2)$, where λ is the neutron radiation wavelength and θ is the scattering angle]. A rectangular quartz cell of 22 × 40 × 2 mm was used.

ANALYTICAL EQUATIONS

The SANS intensity for nonspherical particles is described by (16–22)

$$I(Q) = n_p[\langle F(Q)\rangle^2_{\theta'} S(Q) + \langle |F(Q)|^2\rangle_{\theta'} - \langle F(Q)\rangle^2_{\theta'}], \quad [1]$$

where n_p is the number density of colloidal particles. $F(Q)$ and $S(Q)$ are the particle form factor and the interparticle structure factor, respectively. θ' is an angle between the major axis and the Bragg wavevector. The particle form factor must be averaged over the orientation direction.

Suppose that C is a total molar concentration of surfactant, C_1 is a molar concentration of free monomer and equalized to the critical micelle concentration, and m is an aggregation number of a particle. Then

$$n_p = (C - C_1)N_A/1000m, \quad [2]$$

where N_A is Avogadro's number.

For the dilute solutions involved in this work, the interparticle structure factor can be approximated to be unity. Then the particle form factor contributes to the SANS intensity as a function of Bragg wavenumber:

$$I(Q) = n_p \langle |F(Q)|^2\rangle_{\theta'} \equiv n_p P(Q). \quad [3]$$

$P(Q)$ is the intraparticle structure factor which depends on the particle geometry.

Ellipsoidal Particles

The particle form factor for a monodisperse system of prolate ellipsoidal particles with semimajor and semiminor axes, a and b, is written as

$$F(Q) = 3V(\rho - \rho_s) j_1(u)/u \quad [4]$$

and

$$u = Q[a^2\cos^2\theta' + b^2(1 - \cos^2\theta')]^{1/2}, \quad [5]$$

where $V = 4\pi ab^2/3$ is the total volume of a particle. ρ and ρ_s are the mean coherent neutron scattering length densities of particle and solvent, respectively. $j_1(u)$ is the first-order spherical Bessel function and is described as

$$j_1(u) = (\sin u - u\cos u)/u^2. \quad [6]$$

Then

$$I(Q) = n_p V^2 (\rho - \rho_s)^2 \left| \int_0^1 (3 j_1(u)/u)\, d\cos\theta' \right|^2. \quad [7]$$

When $R_G^2 = (a^2 + 2b^2)/5$ is the square number of radius of gyration and the QR_G value is small, $j_1(u)$ is developed by a small u value. Therefore,

$$I(Q) = n_p V^2 (\rho - \rho_s)^2 \exp(-R_G^2 Q^2/3), \quad [8]$$

which is known as a Guinier equation. It is apparent from Eq. [8] that the logarithmic $I(Q)$ values linearly decrease with increasing Q^2 values.

For homogeneous spherical particles of radius R in a dilute solution, the axes a and b in Eqs. [4]–[8] are replaced by R.

Rigid Rod Particles

For the cylindrical structure of length L and radius R_t of the transversal cross section such that $L \gg R_t$, the SANS intensity is described by

$$QI(Q) = \pi n_p V A_t (\rho - \rho_s)^2 [2 j_1(QR_t)/QR_t]^2 \quad [9]$$

for large QL values. A_t is an area of the transversal cross section of rod. Then $V = LA_t = \pi R_t^2 L$. If the $QR_{G,C}$ value is small,

$$QI(Q) = \pi n_p V A_t (\rho - \rho_s)^2 \exp(-R_{G,C}^2 Q^2/2), \quad [10]$$

where $R_{G,C}$ is the radius of gyration for the transversal cross section and relates to the radius R_t by the equation

$$R_{G,C} = R_t/\sqrt{2}. \quad [11]$$

Equation [10] suggests that a plot of log $QI(Q)$ against Q^2 displays a linear decrease.

Vesicles

Suppose that vesicles are unilamellar and consist of a thin spherical shell with inner and outer radii, R_i and R_o. The SANS intensity is

$$I(Q) = n_p (\rho - \rho_s)^2 [3V_o j_1(QR_o)/QR_o - 3V_i j_1(QR_i)/QR_i]^2, \quad [12]$$

where $V_i = 4\pi R_i^3/3$ and $V_o = 4\pi R_o^3/3$.

In the large QR_G region, where $R_G^2 = 3(R_o^5 - R_i^5)/5(R_o^3 - R_i^3)$,

$$Q^2 I(Q) = 2\pi n_p (A/V) (\rho - \rho_s)^2 (R_o - R_i)^2, \quad [13]$$

where $V = V_o - V_i$ and $A = 4\pi(R_o^2 + R_i^2)$. Relation [13] means that the $Q^2 I(Q)$ values are independent of Q^2 values.

Lamellar Layers

For infinitely extended lamellar layers with the periodic lamellar structure (23),

$$Q^2 I(Q) = 2\pi(t^2/D) (\rho - \rho_s)^2 [\sin(Qt/2)/(Qt/2)]^2, \quad [14]$$

where t is the width of the scattering length density profile. D is a repeat distance of bilayers and calculated from a position Q_{max} of the first-order Bragg peak by using the relation

$$D = t'/\phi = 2\pi/Q_{max}. \quad [15]$$

t' is a bilayer thickness, that is, the width of the mass–density profile, so that $t' \geqslant t$. ϕ denotes a volume fraction of surfactant.

For small $QR_{G,C}$,

$$Q^2 I(Q) = 2\pi(t^2/D) (\rho - \rho_s)^2 \exp(-R_{G,C}^2 Q^2), \quad [16]$$

indicating the linear relation of log $Q^2 I(Q)$ against Q^2. $R_{G,C}$ is the radius of gyration of the thickness t, which is calculated from the relation

$$R_{G,C} = t/\sqrt{12}. \quad [17]$$

RESULTS AND DISCUSSION

C_{12}DAO/Cinnamic Acid/D_2O Ternary System

SANS data for the C_{12}DAO/cinnamic acid/D_2O ternary system at different mixing ratios are illustrated in Fig. 1. Double logarithmic plots of SANS intensity $I(Q)$ and Bragg wavenumber Q displayed the upward curvature for an aqueous C_{12}DAO solution. On the other hand, the logarithmic intensities decreased gradually with log Q for solutions at higher mixing ratios. SANS data were similar for solutions at mixing ratios above 0.5.

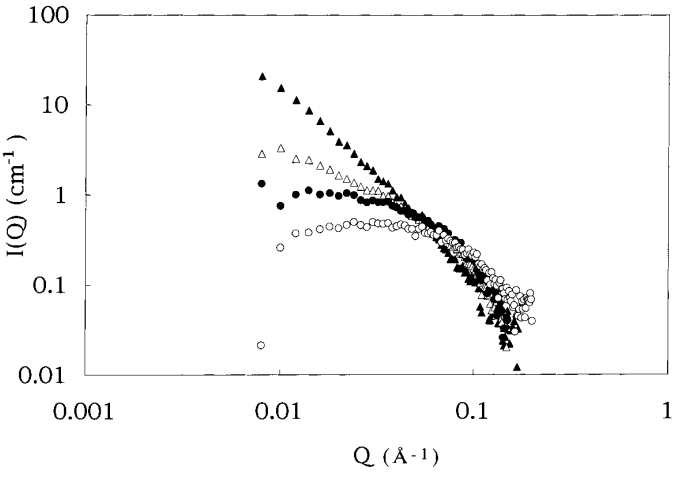

FIG. 1. SANS data for the C_{12}DAO/cinnamic acid/D_2O system. Mixing ratio: ○, $X = 0$; ●, $X = 0.2$; △, $X = 0.4$; ▲, $X = 0.6$.

At $X = 0$ and 0.2. It was proved by light scattering that small micelles formed in an aqueous C_{12}DAO solution without cinnamic acid (8). Small micelles may take the ellipsoidal structure. For small micelles of C_{12}DAO and sodium dodecyl sulfate, the prolate ellipsoid model was more reasonable than the oblate ellipsoid model (24). Then the analytical equations [4]–[8] for the monodisperse prolate ellipsoid were applied to the solution at $X = 0$. The Guinier plot in Fig. 2 (top) showed a linear relation at the wide Q region. The radius of gyration, which was calculated from the tilt on the Guinier plot, was 19 Å.

The SANS intensity at $X = 0.2$ was stronger at smaller Q regions than that at $X = 0$. As seen in Fig. 2 (lower), linearity in the Guinier plot was obtained at $QR_G < 1$, corresponding to the radius of gyration of 27 Å, which was larger than that at $X = 0$. This means that the molecular assemblies in the solution at $X = 0.2$ are larger than those at $X = 0$.

The theoretical SANS intensities evaluated by using variable parameters of a, b, and m were fitted to the observed values. Then the ρ and ρ_s values of 0.011×10^{-12} and 0.064×10^{-12} cm/Å^3, respectively, were used. Optimum theoretical curves for the prolate ellipsoid structure were obtained at $a = 29$ Å and $b = 22$ Å for $X = 0$. From the same procedure, the parameters $a = 52$ Å and $b = 22$ Å were evaluated for $X = 0.2$.

The fully stretched molecular length of C_{12}DAO is 22 Å, which was calculated from the chain length $l_c = 1.5 + 1.265n_c$ at carbon number $n_c = 12$ and head group length 5 Å (24). It is recognized that the semiminor axis of ellipsoidal micelles at $X = 0$ and 0.2 is consistent with the estimated

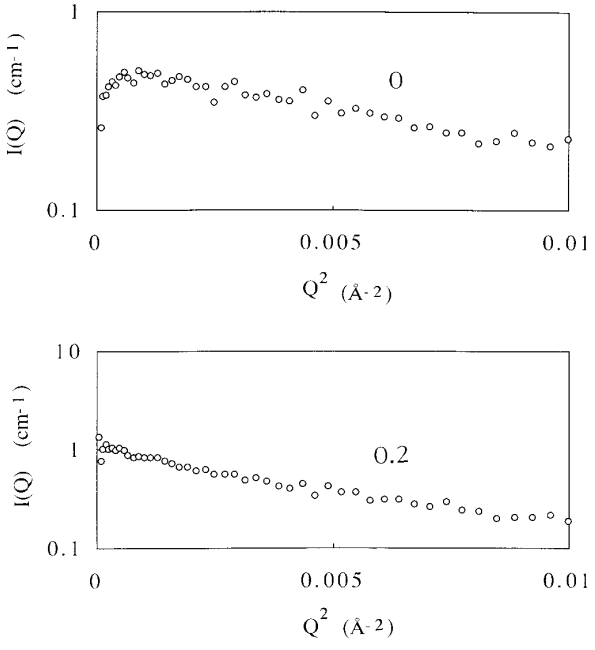

FIG. 2. Replots of SANS data for the C_{12}DAO/cinnamic acid/D_2O system at mixing ratios $X = 0$ and 0.2.

molecular length. Aggregation numbers m obtained from the optimum fitting were 72 and 101 for $X = 0$ and 0.2, respectively. The m values were in good agreement with those obtained from light scattering (15).

The spherical particle model did not reproduce the observed data at $X = 0.2$, suggesting that the particles are not swollen micelles or microemulsions. This supports the idea that a small amount of cinnamic acid acts as a cosurfactant rather than an oil component to form preferably ellipsoidal micelles.

At $X = 0.4$. The solution at $X = 0.4$ is of low viscosity and transparent as are the solutions at $X = 0$ and 0.2. The average mass weight of molecular assemblies evaluated from light scattering was 9.7×10^4, which was only six times larger than that of micelles at $X = 0$ (14). However, TEM observations demonstrated the existence of small vesicles of different sizes and a few larger multilamellar vesicles. Therefore, small micelles and vesicles must coexist in the solution.

The Guinier plot for the solution at $X = 0.4$ did not display linearity, in contrast to the solutions at $X = 0$ and 0.2. On the contrary, the SANS data obeyed the analytial equation for the vesicular structure. Nevertheless, the numerical analysis was not performed, because the contributions of micelles and vesicles had to be considered.

At $X = 0.45-1$. The structure of molecular assemblies in translucent solutions at $X = 0.45-1$ was demonstrated to be vesicles from TEM observations (14). Log Q^2I versus Q^2 plots of SANS data are given in Fig. 3. In the plot for $X = 0.45$, the log Q^2I values were constant against Q^2 values, indicating good adaptation to the analytical equation [13] for vesicles. Although quantitative analysis was attempted under the assumption of vesicles with a unilamellar membrane, the evaluated outer radius did not agree with that from light scattering. The difficulty in the numerical consistency comes from the polydispersity of the vesicular size and shape, the bilayer number, and the interbilayer distance.

The log Q^2I values for solutions at $X = 0.5-1$ decreased linearly with increasing Q^2. This aspect is rather consistent with the analytical equation [16] for lamellar layers. The tendency to decrease was more marked at higher mixing ratios.

With an increase in mixing ratio, vesicles become larger. At the same time, the curveture of bilayers decreases, and the multilamellar layers become predominant in number, as estimated from the TEM results (14). Thus, the macroscopic information for large vesicles cannot be obtained from SANS, but the local lamellar layer thickness and distance can be measured.

From the numerical fitting for the system $X = 1$ on the basis of the lamellar layer structure, a bilayer thickness of 30 Å was evaluated. The same procedure was applied to the solutions at $X = 0.5$, 0.6, and 0.8. The evaluated thickness values were 23, 24, and 27 Å, respectively. The values increased with the mixing ratio, as expected from the adsorp-

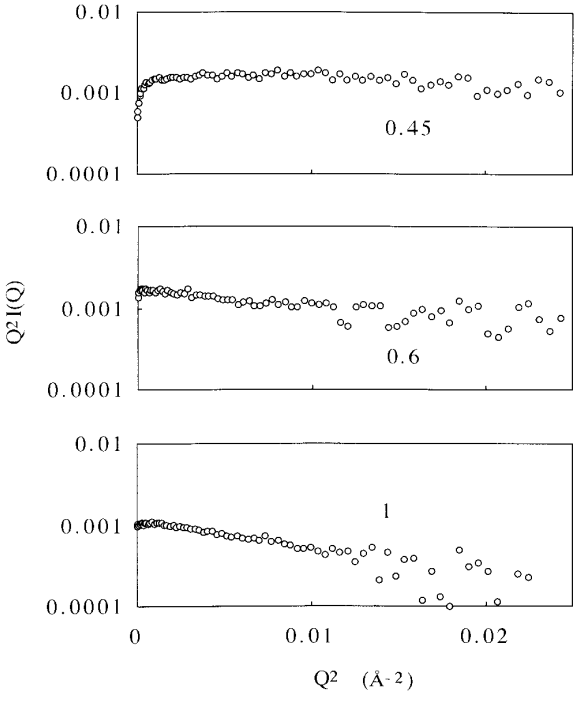

FIG. 3. Replots of SANS data for the C_{12}DAO/cinnamic acid/D_2O system at mixing ratios $X = 0.45$, 0.6, and 1.

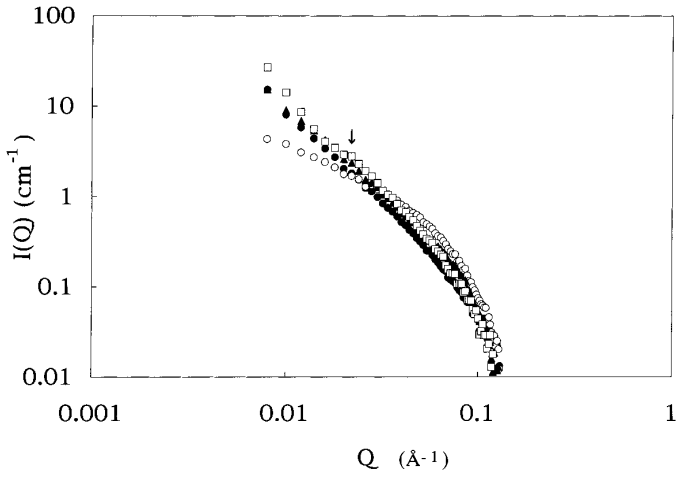

FIG. 4. SANS data for the C_{16}DAO/cinnamic acid/D_2O system. Mixing ratio: ●, $X = 0$; ○, $X = 0.2$; ▲, $X = 0.4$; □, $X = 0.6$.

tion of cinnamic acid on vesicles. However, the absolute values were fairly smaller than the bilayer thickness estimated from the molecular length.

C_{16}DAO/Cinnamic Acid/D_2O Ternary System

Figure 4 shows SANS data for the C_{16}DAO/cinnamic acid/D_2O system at different mixing molar ratios. Double logarithmic plots of intensity and Bragg wavenumber decreased gradually for an aqueous C_{16}DAO solution without cinnamic acid and for the ternary system with mixing ratios above 0.4, whereas the SANS intensity for the solution at $X = 0.2$ decreased more slowly with the initial increase in log Q.

At $X = 0$. It was recognized from video-enhanced microscopic and TEM observations that lamellar layers were formed in a gellike C_{16}DAO solution at $X = 0$ (12, 13). Equations [14]–[17] for the lamellar layer structure were applied to this system. The plot of log $Q^2I(Q)$ versus Q^2 (Fig. 5, top) displayed good linearity with downward tilt, supporting the existence of lamellar layers. The calculated bilayer thickness was 30 Å, which was thinner than the estimated bilayer thickness (53 Å).

At $X = 0.2$. The SANS data for a solution at $X = 0.2$ were applied to the analytical equations for ellipsoids, vesicles, and lamellar layers. However, no structure satisfied the observed intensity. The solution was viscous but transparent, different from the translucent solutions at $X = 0$ and 0.5–1. Such solution character suggests the formation of rodlike micelles. In fact, rodlike micelles are formed in aqueous C_{16}DAO solutions at temperatures higher than 30°C (11, 25). Theoretical equations [9]–[11] derived for rigid rod particles were applied to the observed data.

The plot of log QI versus Q^2 showed good linearity, as seen in Fig. 5 (bottom). The radius of gyration of cross section calculated from the tilt of the plot was 18 Å, which corrsponds to the cross sectional radius of 25 Å. This value is almost consistent with the estimated molecular length, supporting the adequacy of the application of rod structure to molecular assemblies in the solution at $X = 0.2$. Since the linearity of the plot in Fig. 5 (bottom) was realized at very low Q^2 values, the formation of very long rods is suggested (17).

At $X = 0.4$ and 0.45. The existence of vesicles in solutions at $X = 0.4$ and 0.45 was proved by TEM observations (14). There were vesicles of various sizes with uni- to multilamellar layers. The SANS intensity of solutions at $X = 0.4$ and 0.45 submitted reasonably to the analytical equations for visicles; as seen in Fig. 6, the log Q^2I values were constant at low Q^2 values. Comparison of the observed intensity with the calculated intensity was carried out on the basis of Eq. [12] for vesicles with a unilamellar membrane. The calculated outer radius of vesicles was not consistent with the results of light scattering (14), because the size polydispersity and the bilayer multiplicity of vesicles were not considered in this analysis.

At $X = 0.5$–1. Vesicles formed in the solutions at $X = 0.5$–1 were larger and had multilamellar layers (14).

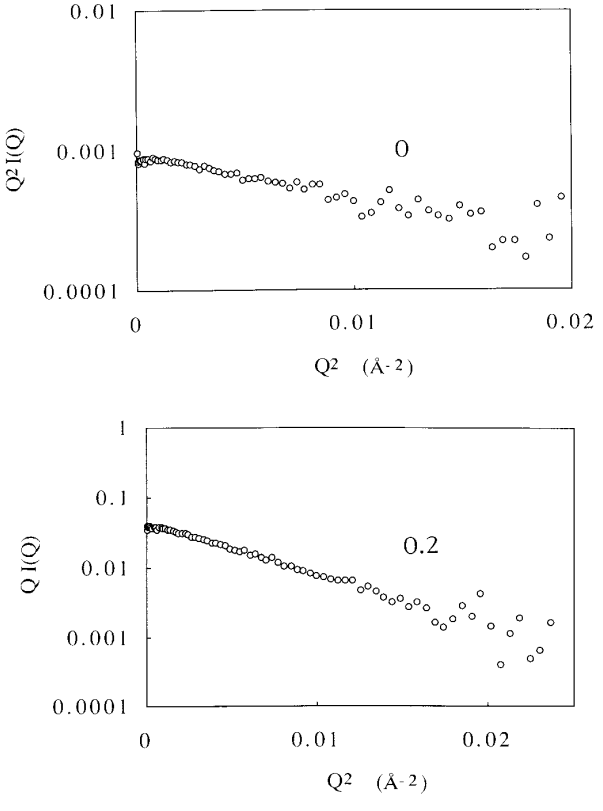

FIG. 5. Replots of SANS data for the C_{16}DAO/cinnamic acid/D_2O system at mixing ratios $X = 0$ and 0.2.

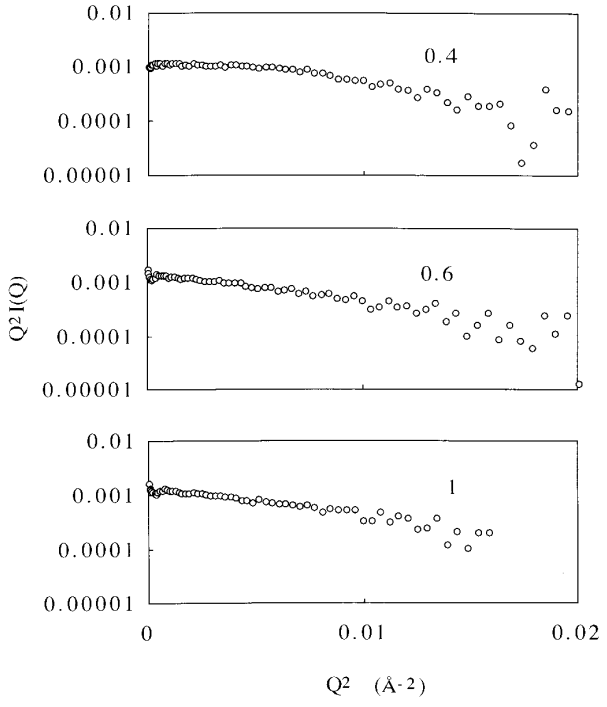

FIG. 6. Replots of SANS data for the C_{16}DAO/cinnamic acid/D_2O system at mixing ratios X = 0.4, 0.6, and 1.

However, their SANS data agreed with the equation for lamellar layers but not for vesicles, for the same reason described for C_{12}DAO/cinnamic acid vesicles at X = 0.5–1: the log Q^2I values decreased linearly with Q^2 values, as seen in Fig. 6.

When the theoretical calculation was compared with the observed SANS intensity by using the lamellar layer model, the bilayer thickness t was evaluated as 35–36 Å. The values are smaller than the bilayer thickness expected.

The SANS curve had a weak peak around Q = 0.03 $Å^{-1}$ for solutions above X = 0.5 (see arrow in Fig. 4). The distance calculated from the observed Bragg peak on the basis of Eq. [15] was 250 Å. This can be assigned to the average distance between bilayers.

Molecular Assemblies in a C_nDAO/Cinnamic Acid/Water System

Macroscopic structures of molecular assemblies formed in the C_nDAO/cinnamic acid/water ternary system vary with changes in the mixing molar ratio of cinnamic acid to C_nDAO (14, 15). In this work, the structures were quantitatively determined on a microscopic scale from analysis of the SANS intensity based on the models of ellipsoidal micelles, rodlike micelles, vesicles, and lamellar layers. The evaluated numerical values of structural parameters for molecular assemblies are listed in Table 1. Figure 7 illustrates the schematic representation of possible models of molecular assemblies in the C_nDAO/cinnamic acid/water ternary system.

In the C_{12}DAO/cinnamic acid/water ternary system, prolate ellipsoidal micelles with a semiminor axis of 22 Å were

TABLE 1
Structural Parameters for Molecular Assemblies in the C_nDAO/Cinnamic Acid/Water System

X	m	R_G (Å)	a (Å)	b (Å)	$R_{G,C}$ (Å)	R_t (Å)	$t/2$ (Å)	D (Å)	Structure
				C_{12}DAO/cinnamic acid/water					
0	72	19	29	22					Ellipsoidal micelle
0.2	101	27	52	22					Ellipsoidal micelle
0.4									Micelle + Vesicle
0.45									Vesicle
0.5							11.5		Multilamellar vesicle
0.6							12		Multilamellar vesicle
0.8							13.5		Multilamellar vesicle
1							15		Multilamellar vesicle
				C_{16}DAO/cinnamic acid/water					
0							15		Lamellar layer
0.2					18	25			Rodlike micelle
0.4									Vesicle
0.45									Vesicle
0.5							17.5	250	Multilamellar vesicle
0.6							18	250	Multilamellar vesicle
0.8							18	250	Multilamellar vesicle
1							17.5	250	Multilamellar vesicle

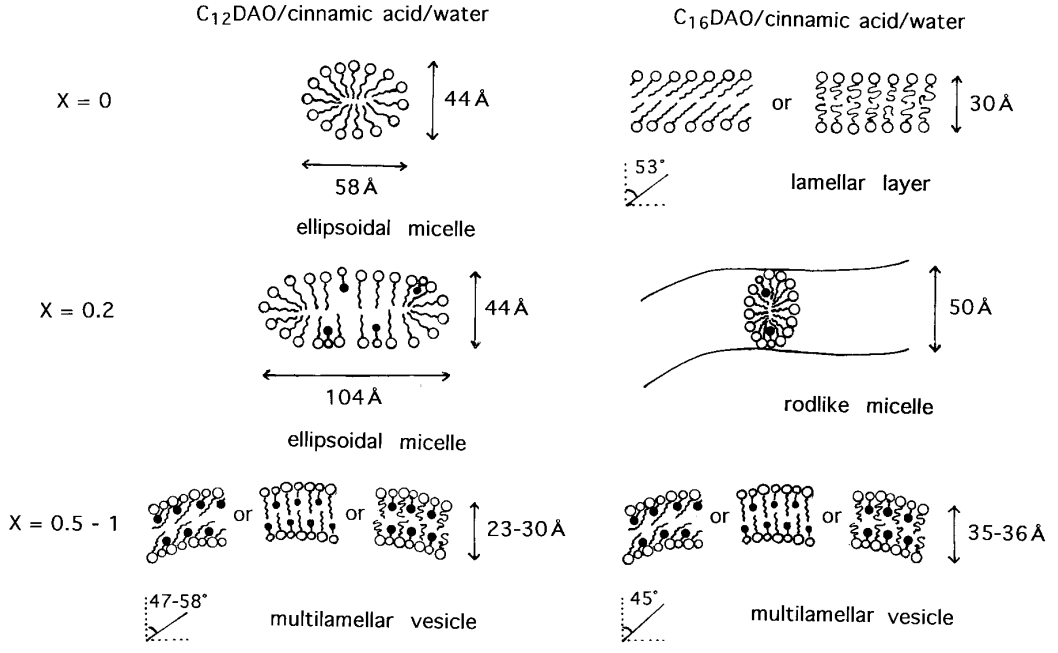

FIG. 7. Schematic representation of possible models for the molecular assemblies of the C_nDAO/cinnamic acid complexes.

formed at $X = 0$ and 0.2. Their semimajor axes were 29 and 52 Å for $X = 0$ and 0.2, respectively. For multilamellar vesicles formed in the solutions at higher mixing ratios, bilayer thicknesses of 23–30 Å were evaluated.

In the C_{16}DAO/cinnamic acid/water system, the thickness of lamellar layers in the solution at $X = 0$ was 30 Å. Long rodlike micelles at $X = 0.2$ had a cross-sectional diameter of 50 Å. At higher mixing ratios, there were vesicles with bilayer thicknesses of 35–36 Å and an interlamellar distance of 250 Å.

The semiminor axis of ellipsoidal micelles obtained in the C_{12}DAO/cinnamic acid/water system at $X = 0$ and 0.2 was in good agreement with the estimated molecular length, as well as the cross-sectional radius of rodlike micelles in the C_{16}DAO/cinnamic acid/water system at $X = 0.2$. However, the membrane bilayer thickness of multilamellar vesicles in the C_nDAO/cinnamic acid/water systems at $X = 0.5–1$ was fairly smaller than the theoretical estimation. A smaller thickness was also obtained for lamellar layers in the C_{16}DAO solution without cinnamic acid ($X = 0$). Thus, the tilt of alkyl chains or their random orientation may occur in bilayers. It is also possible that pairs of C_nDAO and cinnamic acid molecules arrange in a comb shape in membrane bilayers of C_nDAO/cinnamic acid vesicles. The tilt angles of alkyl chains in the first model were 45–58°.

The smaller bilayer thickness indicates that cinnamic acid is intercalated mainly into bilayers of vesicles, but does not bind to bilayer surfaces. Since C_nDAO and cinnamic acid are a weak base and acid, respectively, they are protonated with opposite sign in water so that they form ion pairs. Cinnamic acids that bind electrostatically with C_nDAO are located near the palisade of bilayers by directing aromatic groups toward the interior of the bilayer, as illustrated in Fig. 7. With respect to the photochemical reaction of cinnamic acid, the cyclodimerization occurs between intercalated molecules oriented paralell to each other. In fact, head-to-head dimer species were dominant over head-to-tail species in vesicular solutions (14).

REFERENCES

1. Wolff, T., and Muller, N., *J. Photochem.* **23,** 131 (1983); **22,** 61 (1983).
2. Takagi, K., Miyake, N., Nakamura, E., Usami, H., and Sawaki, Y., *J. Chem. Soc. Faraday Trans. 1* **84,** 3475 (1988).
3. Ueno, A., Moriwaki, F., Iwama, Y., Suzuki, I., Osa, T., Ohta, T., and Nozoe, S., *J. Am. Chem. Soc.* **113,** 7034 (1991).
4. Takagi, K., Suddaby, B. R., Vadas, S. L., Backer, C. A., and Whitten, D. G., *J. Am. Chem. Soc.* **108,** 7865 (1986).
5. Takagi, K., Fukaya, H., Miyake, N., and Sawaki, Y., *Chem. Lett.*, 1053 (1988).
6. Takagi, K., Nambara, E., Usami, H., Itoh, M., and Sawaki, Y., *J. Chem. Soc. Perkin Trans. 1,* 655 (1991).
7. Takagi, K., Itoh, M., Usami, H., Imae, T., and Sawaki, Y., *J. Chem. Soc. Perkin Trans. 2,* 1003 (1994).
8. Ikeda, S., Tsunoda, M., and Maeda, H., *J. Colloid Interface Sci.* **70,** 448 (1979).
9. Abe, A., Imae, T., Shibuya, A., and Ikeda, S., *J. Surf. Sci. Technol.* **4,** 67 (1988).
10. Okamura, H., Imae, T., and Furusaka, M., *J. Colloid Interface Sci.* **168,** 217 (1994).

11. Imae, T., Sasaki, M., and Ikeda, S., *J. Colloid Interface Sci.* **131,** 601 (1989).
12. Imae, T., and Trend, B., *J. Colloid Interface Sci.* **145,** 207 (1991).
13. Imae, T., and Iwamoto, T., *J. Colloid Interface Sci.* **152,** 289 (1991).
14. Imae, T., Tsubota, T., Okamura, H., Mori, O., Takagi, K., Itoh, M., and Sawaki, Y., *J. Phys. Chem.* **99,** 6046 (1995).
15. Imae, T., Mori, O., Takagi, K., Itoh, M., and Sawaki, Y., *Colloid Polym. Sci.* **273,** 579 (1995).
16. Guinier, A., Fournet, G., ''Small Angle Scattering of X-rays.'' Wiley, New York, 1955.
17. Glatter, O., and Kratky, O., ''Small Angle X-ray Scattering.'' Academic Press, San Diego, 1982.
18. Chen, S. H., *Annu. Rev. Phys. Chem.* **37,** 351 (1986).
19. Chen, S. H., and Lin, T. L., *Methods Exp. Phys.* **23,** 489 (1987).
20. Feigin, L. A., and Svergun, D. I., ''Structure Analysis by Small-Angle X-ray and Neutron Scattering'' (G. W. Taylor, Ed.). Plenum, New York/London, 1987.
21. Lindner, P., and Zemb, Th. (Eds.), ''Neutron, X-ray and Light Scattering: Introduction to an Investigative Tool for Colloidal and Polymeric Systems.'' North-Holland, Amsterdam, 1991.
22. Schurtenberger, P., Magid, L. J., King, S. M., and Lindner, P. J., *J. Phys. Chem.* **95,** 4173 (1991).
23. Strey, R., Schomacker, R., Roux, D., Nallet, F., and Olsson, U., *J. Chem. Soc. Faraday Trans.* **86,** 2253 (1990).
24. Kakitani, M., Imae, T., and Furusaka, M., *J. Phys. Chem.* **99,** 16–18 (1995).
25. Hashimoto, K., and Imae, T., *Langmuir* **7,** 1734 (1991).